

Dynamic X-ray Spectroscopy of $\rm La_{0.6}Sr_{0.4}CoO_{3-\delta}$ Thin Film Electrodes

To cite this article: Brian S Gerwe et al 2019 ECS Trans. 91 1387

View the <u>article online</u> for updates and enhancements.

ECS Transactions, 91 (1) 1387-1395 (2019) 10.1149/09101.1387ecst ©The Electrochemical Society

Dynamic X-ray Spectroscopy of La_{0.6}Sr_{0.4}CoO_{3-δ} Thin Film Electrodes

B.S. Gerwe^a, K. Mizuno^b, O. Sekizawa^c, K. Nitta^c, K. Amezawa^b, S.B. Adler^a

Dense thin films of the solid oxide fuel cell cathode material La_{0.6}Sr_{0.4}CoO_{3- δ} were studied by *operando* X-ray absorption spectroscopy under sinusoidal voltage perturbations. This approach showed good agreement with previous steady-state μ -XAS measurements, but with high effective $p(O_2)$ resolution over several orders of magnitude. Co oxidation state varied strongest under a 0.5 Hz perturbation suggesting, in agreement with linear impedance, that oxygen exchange kinetics are most active at this timescale. Furthermore, the local structure around Co atoms response varied at different timescales; however, interpretation was limited with only preliminary analysis. Altogether, this approach was shown as a successful step towards developing a technique sensitive to local chemical state that can also separate processes by timescale.

Introduction

Transition-metal oxide perovskites are promising for use solid oxide fuel cell (SOFC) electrodes, gas sensors, oxygen separation devices and ceramic membranes reactors. Their promise arises from mixed electronic and ionic conducting properties which extends the electrochemically active portion of an electrode by providing an oxygen vacancy transport pathway. In particular $La_{1-x}Sr_xCoO_{3-\delta}$ has been widely studied as an oxygen electrode for its high oxygen ion conductivity and large nonstoichiometry at intermediate temperatures leading to a general understanding of the bulk thermodynamics (1,2). However, previous work showed bulk material used for porous electrodes behaves substantially different than thin film electrodes used to isolate kinetics, pointing to possible differences in *local* thermodynamics (3–5). This necessitates development of techniques sensitive to local chemistry with access to temperatures and gas environments relevant to SOFC operation. Furthermore, the ability to selectively probe processes based on time scale, as with impedance spectroscopy, is highly advantageous. This work demonstrates the first step towards such a technique extending previous developments of *operando* micro XAS (*operando* μ -XAS) to the frequency domain (6–8).

XAS is a useful tool for investigating high temperature material *in situ* as it does not require specific experimental conditions and provides extensive element-specific information about the chemical and physical environment around a probe atom (9). The absorption edge of a transition-metal is highly sensitive to electronic state, which is closely correlated to its mean oxidation state, resulting in positive energy shifts at higher

^a Department of Chemical Engineering, University of Washington, Seattle, Washington 98195, USA

^b Institute of Multidisciplinary Research for Advanced Materials, Tohoku University, 2-1-1 Katahira, Aoba-ku, Sendai 980-8577, Japan

^c Japan Synchrotron Radiation Research Institute, 1-1-1 Koto, Sayo 679-5198, Japan

mean valence states (6,10). The mean valence state of Co in LSC shifts to compensate for oxygen vacancies introduced by the following defect equilibrium expressed in Kröger-Vink notation:

$$O_0^X + 2Co_{Co}^{\bullet} \rightleftharpoons \frac{1}{2}O_2(g) + V_0^{\bullet \bullet} + 2Co_{Co}^X$$
 [1]

Therefore, the oxygen chemical potential can be effectively measured by energy shifts in the Co K-edge absorption spectra, where shifts to lower energy indicate lower oxygen potential and partial reduction of the oxide.

Experimental

Thin Film Electrochemical Cell

Dense thin film electrochemical cells were synthesized by Keita Mizuno and coworkers at Tohoku University. Approximately 3g of Ce_{0.9}Gd_{0.1}O_{1.95} powder (GDC, Shin-Etsu Chemical Co., Ltd.) was uniaxially pressed in 20 mm diameter die followed by hydrostatic pressing at 200 MPa. The pellet was then sintered at 1550 °C for 5 hours to produce an approximately 3 mm thick pellet with an approximate diameter of 16 mm and 97% of theoretical density. One side of the pellet was mirror-polished (performed by Disco, Inc.) to an average surface roughness of 2.0-5.0 nm. A counter electrode was painted on the unpolished surface by mixing Pt paste (Tanaka Kikinzoku Kogyo Co., Ltd.) and LSC64 powder (AGC Seimi Chemi) in a 6:4 weight ratio. The counter electrode was then fired at 950 °C for 3 hours. A thin film electrode was then deposited on the polished side of the pellet by pulsed laser deposition (PLD, YAG laser, 180 mW) under 10⁻⁵ bar O₂ and a substrate temperature of 800 °C. The thin film was then annealed at 800 °C for 4 hours under 1 bar O₂. The resulting film was approximately 570 nm thick and 13 mm in diameter. Finally, the sample was cut down a cube roughly 3 x 3 x 3 mm in size and a Pt reference electrode was painted around the bare sides.

Electrochemical impedance spectroscopy (EIS) was measured potentiodynamically using a Bio-Logic SP-150 potentiostat with a 20 mV perturbation amplitude with frequencies spanning 1 kHz to 17 mHz. Measurements were collected while the sample was in an *operando* micro XAS holder, as detailed in (7,11) , under a 10% $\rm O_2$ balance $\rm N_2$ gas environment at 973 K.

Dynamic operando X-ray Absorption Spectroscopy (XAS)

Using a custom built sample holder fabricated by co-workers at Tohoku University, fluorescence mode XAS measurements were carried out at the BL37XU beam line, Spring-8, JASRI, Japan (7,11). At this beam line, the incident X-ray can be focused to a micro or sub-micrometer spot size using a Karkpatric-Baez mirror. Incident X-ray energies spanned 7600 eV to 7845 eV. Fluoresced X-rays were collected by a photodiode and incident X-rays were collected by an ion chamber. Analog signals from the fluoresced and incident X-rays were collected synchronously with current and voltage signals from the SP-150 potentiostat by two National Instruments 5922 oscilloscopes. Custom LabVIEW software was written to carry out the measurements.

Results and Discussion

Electrochemical Impedance Spectroscopy (EIS)

Figure 1 shows the EIS spectrum collected at 973 K in 10% O_2 with no applied bias. A slightly depressed semi-circle is observed indicating the electrode is kinetically limited. A simplified Randles circuit with a constant phase element was fit to the data resulting in values of 64.2 Ω , 47.2 Ω , 9.41x10⁻³ F·s^{0.935} for R_s, R_c, and CPE, respectively. This approach is used primarily to facilitate frequency-dependent overpotential calculations for the voltage perturbations according to:

$$\eta(t) = \tilde{V}(t) - i(t)R_s \tag{2}$$

Dynamic operando X-ray Absorption Spectroscopy

Figure 2 shows Co K-edge X-ray absorption spectra observed for the LSC electrode at 973 K in 10% O₂ at many points (overpotentials) along a perturbation cycle for applied frequencies 0.5, 1, and 5 Hz. Note the spectra have not been normalized and flattened to pre-edge and post-edge lines. At cathodic (negative) overpotentials, the absorption edge shifts towards lower energies relative to the unbiased state, whereas at anodic (positive) overpotentials the edge shifts to higher energies. These results qualitatively agree with previous steady-state measurements connecting Co absorption edge shifts to changes in mean Co oxidation state to compensate oxygen vacancy concentration shifts (6,10,11). As the perturbation frequency increases the absorption edge excursions narrow and the range of overpotentials also decreases. The latter is a consequence of controlling total cell voltage.

Figure 3 shows the relative (mean subtracted) absorbance at 7720 eV incident Xray energy for all three perturbation frequencies as functions of the applied overpotential where positive values indicate absorption edge shifts to lower energies. The trends for absorbance excursions and overpotential range seen in Figure 2 hold true here as this is simply another perspective on the same data. The slope is lowest for 5 Hz and highest for 0.5 Hz, though the 0.5 Hz and 1 Hz slopes are nearly identical. These slopes relate how strongly the XAS spectra is shifting independent of the overpotential range. Theoretically the absorbance should fall on a single line as the overpotential sweeps through a perturbation cycle; however, the data have some ellipsoidal character. One explanation is a phase lag arising from bulk vacancy diffusion through the film thickness and the volume-averaged nature of XAS measurements. As the vacancy concentration at the electrolyte/electrode interface is modulated by the overpotential, vacancies must diffuse through the film to the gas-exposed surface. When the characteristic time for diffusion isn't fast compared to the perturbation, a concentration profile develops perpendicular to the film resulting in dissimilar absorbances at a given overpotential depending on the cycle phase. Using the 570 nm electrode thickness and assuming a vacancy diffusion coefficient of 10⁻⁷ cm²/s gives rise to a characteristic diffusion time of 32.5 ms (12). This time corresponds to phase lags of 5.9, 11.7, and 58.5° for the 0.5, 1, and 5 Hz perturbations, respectively. In accordance with this theory 1 Hz is wider than 0.5 Hz; however, 5 Hz does not open as expected.

The narrow absorbance excursions and small slope for 5 Hz seen in Figure 2 and Figure 3, respectively, indicate only small shifts in the Co valence state and therefore oxygen potential in the oxide. Since 5 Hz is close to the high-frequency intercept in Figure 1, this suggests the timescale is too fast to significantly activate oxygen kinetics. On the other hand, the 0.5 and 1 Hz perturbations show the wide excursions in Figure 2 and high slopes in Figure 3 indicating the oxygen potential is modulated considerably. Again, these results are consistent with EIS in Figure 1, where 0.5 and 1 Hz are considerably higher on the depressed semicircle suggesting oxygen kinetics are engaged at those timescales. In fact, the XAS results support the impedance interpretation as it represents a direct measure of the faradaic reaction.

Local Structure

Figure 4. Magnitude of Fourier transformed XAS around Co atoms in La0.6Sr0.4CoO3- δ under a) 0.5 Hz, b) 1 Hz, and c) 5 Hz voltage perturbations in 10% O2 at 973 K. Lines represent the RDF at a single overpotential in the sinusoidal perturbation, as indicated by color where red are anodic (positive) and blue are cathodic (negative) overpotentials. Figure 4 shows the magnitude of Fourier transformed XAS weighted by k^2 (FT[$|\chi k^2|$]) around the Co atom in LSC64. This reveals the coordination and bonding distances around Co from photoelectron scattering by neighboring atoms (9). Lateral shifts in peak position indicate changes in bond length while shifts in intensity may relate to electron density around the absorbing Co atom (9). The peaks around 1-2 Å are attributed to first neighbor Co-O pairs whereas peaks around 3-4 Å correspond to second neighbor Co-(La,Sr) and third neighbor Co-Co pairs.

As with Figure 2, each line represents the $FT[|\chi k^2|]$ for a single overpotential in the perturbation cycle. The $FT[|\chi k^2|]$ peaks around 1.5 Å for 5 Hz are essentially insensitive to the overpotential, whereas those for 0.5 Hz and 1 Hz significantly shift in amplitude. Notably, the peaks do not observably shift laterally, indicating bond lengths are effectively unchanged despite observable oxidation state shifts in Figure 2. This disparity is rationalized by chemical expansion in LSC which arises from changes in Co-O bond length as vacancies are introduced to the material (13). Uniaxial strain for an isotropic solid is given by

$$d\varepsilon = \frac{1}{3}\beta_t dT + \frac{1}{3}\beta_c dx_v$$
 [3]

where ε , β_t , T, β_c , and x_v are the uniaxial strain, thermal expansivity, temperature, chemical expansivity, and oxygen vacancy mole fraction, respectively. Let us consider isothermal strain arising from chemical expansion taking $\frac{1}{3}$ $\beta_c \approx 0.1$ ppm/ppm (13,14). The shift in x_v for 0.5 Hz is estimated to be $\sim 8\%$ from $\partial \ln x_v = (-1/2 A) \partial \ln P_{O_2}$ with $\partial \ln P_{O_2} = -5$, and assuming A ≈ 2 and $x_{v,o} = 0.02$. Therefore, the estimated shift in bond length is only 0.8%! Moreover, if the film is not diffusionally equilibrated, as suggested earlier, the peak would broaden at intermediate frequencies and obscure small shifts in the peak position.

On the other hand, the peak amplitude modulations may arise from changes in the scattering properties of the photoelectron (i.e. electron density surrounding Co) or Co coordination; however, distinguishing between these effects is complicated due to correlation of the factors (9). If we assume coordination number changes are dominant,

the 4% amplitude shift, and therefore coordination number, for 0.5 Hz only accounts for 0.7% change in x_v . The inconsistency motivates further analysis of χ , including modeling X-ray Absorption Fine Structure spectra; however, such analysis is beyond the scope of this work.

Conclusions

Dynamic changes in the electronic and local structures of $La_{0.6}Sr_{0.4}CoO_{3-\delta}$ dense thin films were studied by measuring Co K-edge XAS during sinusoidal voltage perturbations. Absorption edge shifts qualitatively agreed with previous works; however, this approach revealed smooth transitions in Co oxidation state over several orders of magnitude in $p(O_2)$. Different timescales of processes were probed by varying the voltage perturbation frequency showing oxygen kinetics respond strongest at 0.5 Hz in agreement with EIS results. Although the Co-O bond length changes with oxygen vacancy concentration, such shifts in local structure were immeasurable in the Fourier transformed XAS. Amplitude shifts observed in the local structure were inconsistent with changes in Co coordination; however, further analysis is required to deduce the cause. Altogether, it was shown this approach can be used to study and separate dynamic changes in electronic and local structures of high temperature materials by timescale.

Acknowledgments

The authors would like to thank the National Science Foundation and the Japan Science and Technology Agency for financially supporting this work.

References

- 1. S. B. Adler, *Chem Rev.*, **104**(10), 4791–844 (2004).
- 2. J. Mizusaki, Y. Mima, S. Yamauchi, K. Fueki, and H. Tagawa, *Journal of Solid State Chemistry.*, **80**(1), 102–11 (1989).
- 3. J. R. Wilson, M. Sase, T. Kawada, and S. B. Adler, *Electrochem Solid-State Lett.*, **10**(5), B81–6 (2007).
- 4. C. R. Kreller, T. J. McDonald, S. B. Adler, E. J. Crumlin, E. Mutoro, S. J. Ahn, et al., J Electrochem Soc., **160**(9), F931–42 (2013).
- 5. T. Kawada, J. Suzuki, M. Sase, A. Kaimai, K. Yashiro, Y. Nigara, et al., J Electrochem Soc., 149(7), E252–9 (2002).
- 6. K. Amezawa, Y. Orikasa, T. Ina, A. Unemoto, M. Sase, H. Watanabe, *et al.*, *ECS Trans.*, **13**(26), 161–4 (2008).
- 7. K. Amezawa, Y. Fujimaki, T. Nakamura, K. D.- Bagarinao, K. Yamaji, K. Nitta, *et al.*, *ECS Trans.*, **66**(2), 129–35 (2015).
- 8. K. Amezawa, Y. Fujimaki, K. Mizuno, Y. Kimura, T. Nakamura, K. Nitta, *et al.*, *ECS Trans.*, **77**(10), 41–7 (2017).
- 9. M. Newville, *Reviews in Mineralogy and Geochemistry.*, **78**(1), 33–74 (2014).
- 10. Y. Orikasa, T. Ina, T. Nakao, A. Mineshige, K. Amezawa, M. Oishi, *et al.*, *J Phys Chem C.*, **115**(33), 16433–8 (2011).
- 11. Y. Fujimaki, H. Watanabe, Y. Terada, T. Nakamura, K. Yashiro, S. Hashimoto, *et al.*, *ECS Trans.*, **57**(1), 1925–32 (2013).

- 12. Y. Lu, C. Kreller, and S. B. Adler, *J Electrochem Soc.*, **156**(4), B513–25 (2009).
- 13. S. B. Adler, Journal of the American Ceramic Society., 84(9), 2117–9 (2001).
- 14. Y. Ohno, S. Nagata, and H. Sato, *Solid State Ionics.*, **9–10**, 1001–7 (1983).

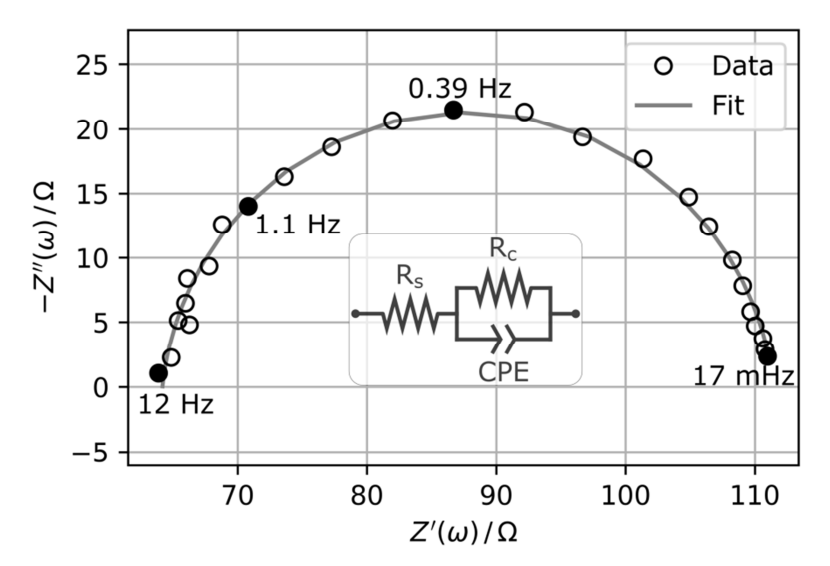


Figure 1. The EIS spectrum of the thin film at 973 K in 10% O_2 shows a slightly depressed semi-circular shape, suggesting kinetic limitations. Data is fit to the simple Randles circuit shown in the inset.

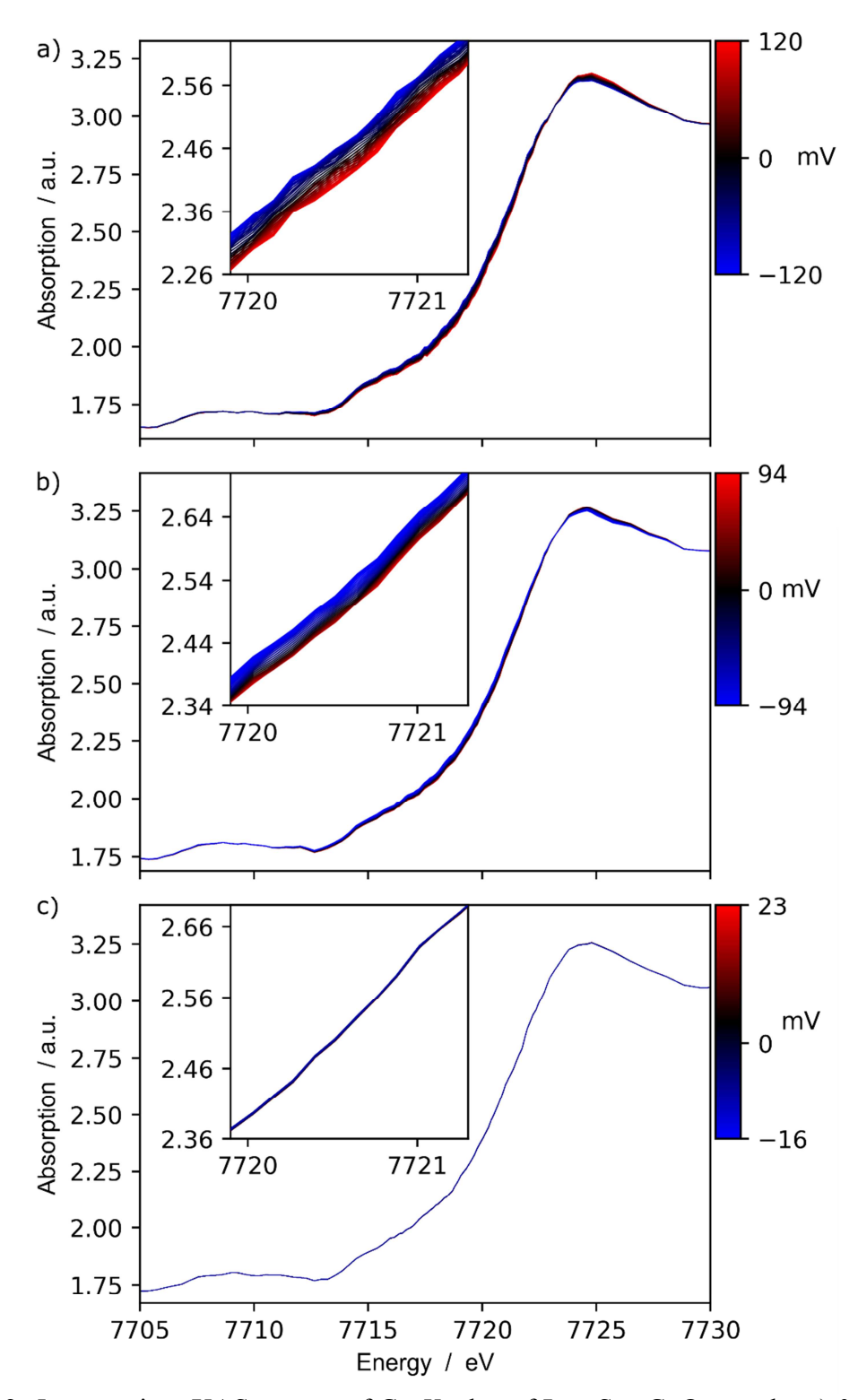


Figure 2. *In-situ* micro XAS spectra of Co K-edge of La_{0.6}Sr_{0.4}CoO_{3- δ} under a) 0.5 Hz, b) 1 Hz, and c) 5 Hz voltage perturbation in 10% O₂ at 973 K. Lines represent the spectrum at a single overpotential in the sinusoidal perturbation, as indicated by color where red are anodic (positive) and blue are cathodic (negative) overpotentials.

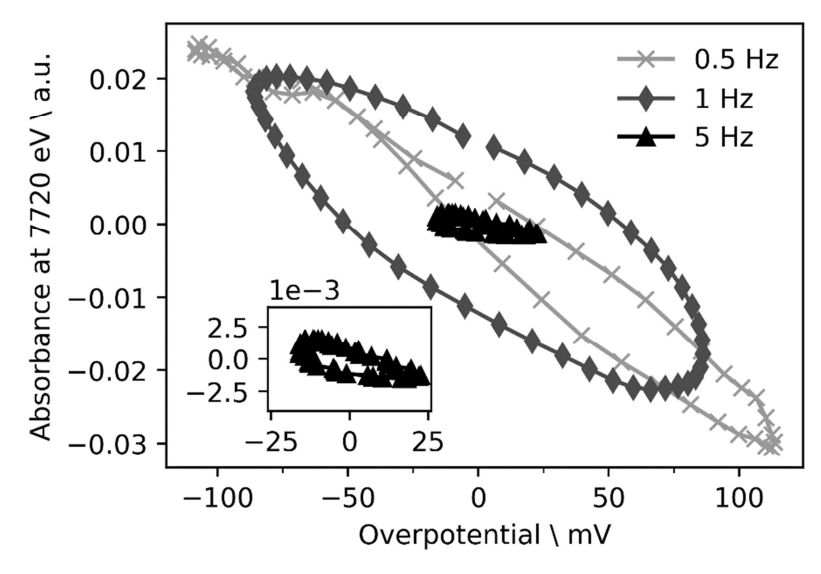


Figure 3. Relative X-ray absorbance at 7720 eV incident X-ray energy for 0.5, 1 and 5 Hz voltage perturbation frequencies. Inset is an expanded view of 5 Hz data.

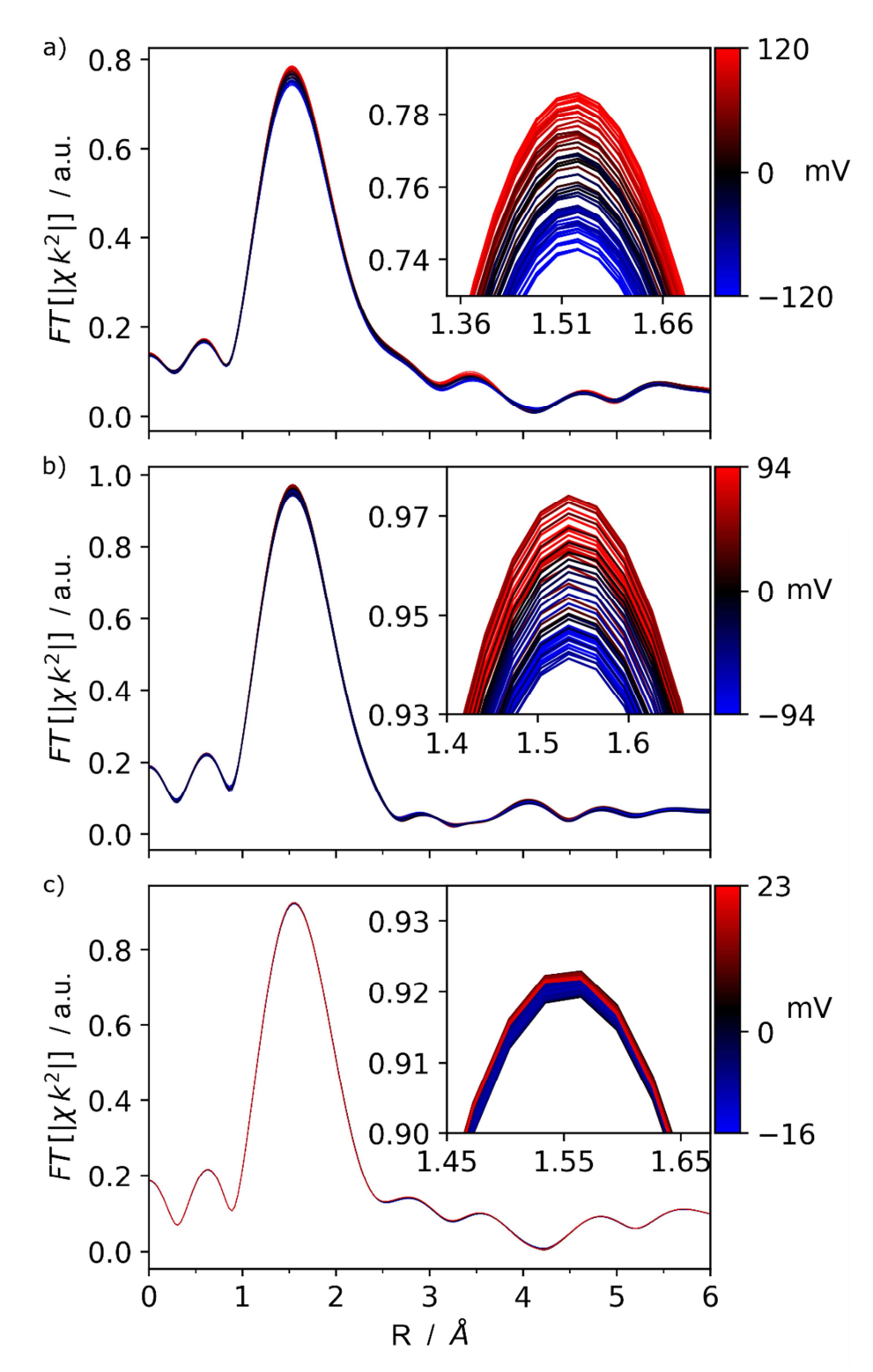


Figure 4. Magnitude of Fourier transformed XAS around Co atoms in $La_{0.6}Sr_{0.4}CoO_{3-\delta}$ under a) 0.5 Hz, b) 1 Hz, and c) 5 Hz voltage perturbations in 10% O_2 at 973 K. Lines represent the RDF at a single overpotential in the sinusoidal perturbation, as indicated by color where red are anodic (positive) and blue are cathodic (negative) overpotentials.